Aerosol and Air Quality Research, 15: 2037–2050, 2015

ISSN: 1680-8584 print / 2071-1409 online
doi: 10.4209/aaqr.2015.05.0310

Vertical Distribution and Columnar Optical Properties of Springtime Biomass-Burning Aerosols over Northern Indochina during 2014 7-SEAS Campaign

Sheng-Hsiang Wang[1*], Ellsworth J. Welton[2], Brent N. Holben[2], Si-Chee Tsay[2], Neng-Huei Lin[1], David Giles[2,3], Sebastian A. Stewart[2,3], Serm Janjai[4], Xuan Anh Nguyen[5], Ta-Chih Hsiao[6], Wei-Nai Chen[7], Tang-Huang Lin[8], Sumaman Buntoung[4], Somporn Chantara[9], Wan Wiriya[9]

[1] *Department of Atmospheric Sciences, National Central University, Taoyuan, Taiwan*
[2] *Goddard Space Flight Center, NASA, Greenbelt, Maryland, USA*
[3] *Science Systems and Applications, Inc., Lanham, Maryland, USA*
[4] *Department of Physics, Faculty of Science, Silpakorn University, Nakhon Pathom, Thailand*
[5] *Institute of Geophysics, Vietnam Academy of Science and Technology, Hanoi, Viet Nam*
[6] *Graduate Institute of Environmental Engineering, National Central University, Taoyuan, Taiwan*
[7] *Research Center for Environmental Changes, Academia Sinica, Taipei, Taiwan*
[8] *Center for Space and Remote Sensing Research, National Central University, Taoyuan, Taiwan*
[9] *Chemistry Department and Environmental Science Program, Faculty of Science, Chiang Mai University, Chiang Mai, Thailand*

ABSTRACT

In this study, the aerosol optical properties and vertical distributions in major biomass-burning emission area of northern Indochina were investigated using ground-based remote sensing (i.e., four Sun-sky radiometers and one lidar) during the Seven South East Asian Studies/Biomass-burning Aerosols & Stratocumulus Environment: Lifecycles & Interactions Experiment conducted during spring 2014. Despite the high spatial variability of the aerosol optical depth (AOD; which at 500 nm ranged from 0.75 to 1.37 depending on the site), the temporal variation of the daily AOD demonstrated a consistent pattern among the observed sites, suggesting the presence of widespread smoke haze over the region. Smoke particles were characterized as small (Ångström exponent at 440–870 nm of 1.72 and fine mode fraction of 0.96), strongly absorbing (single-scattering albedo at 440 nm of 0.88), mixture of black and brown carbon particles (absorption Ångström exponent at 440–870 nm of 1.5) suspended within the planetary boundary layer (PBL). Smoke plumes driven by the PBL dynamics in the mountainous region reached as high as 5 km above sea level; these plumes subsequently spread out by westerly winds over northern Vietnam, southern China, and the neighboring South China Sea. Moreover, the analysis of diurnal variability of aerosol loading and optical properties as well as vertical profile in relation to PBL development, fire intensity, and aerosol mixing showed that various sites exhibited different variability based on meteorological conditions, fuel type, site elevation, and proximity to biomass-burning sources. These local factors influence the aerosol characteristics in the region and distinguish northern Indochina smoke from other biomass-burning regions in the world.

Keywords: Aerosol optical properties; Smoke haze; Biomass burning; Lidar; Seven South East Asian Studies (7-SEAS).

INTRODUCTION

Recent studies have emphasized that the biomass-burning emissions from Indochina considerably influence the regional air quality, long-range transport, cloud formations, atmospheric radiation, hydrological cycle, carbon cycle, and climate (e.g., Reid *et al.*, 2012; Lin *et al.*, 2013; Tsay *et al.*, 2013; Lin *et al.*, 2014). These observations were based on satellite observations (e.g., Hsu *et al.*, 2003; Huang *et al.*, 2011; Campbell *et al.*, 2013; Feng and Christopher, 2013), surface remote sensing (Gautam *et al.*, 2013), *in situ* measurements (Tsai *et al.*, 2012; Chuang *et al.*, 2013; Li *et al.*, 2013), and modeling studies (Fu *et al.*, 2012) within the Seven South East Asian Studies (7-SEAS) framework. However, ground-based measurements, which can provide strong evidence to support the rationale that biomass-burning activities have extensive regional influences, remain limited

* Corresponding author.
Tel.: +886-3-422-7151 ext. 65527
E-mail address: shenghsiang.wang@gmail.com; carlo@cc.ncu.edu.tw

for this region.

The biomass-burning activities in the Indochina peninsula are possibly attributable to the burning of forests and agricultural residue (e.g., Hao and Liu, 1994; Streets *et al.*, 2003). According to the emission inventory for Asian biomass burning reported by Streets *et al.* (2003), Indochina has a strong seasonal variation in the amount of emissions, with the highest emissions occurring in March; furthermore, this report indicated that forest burning is the largest contributor to such emissions. Gautam *et al.* (2013) also reported that considerable biomass-burning activities (i.e., satellite fire spots) encompassing Myanmar, Laos, and Thailand reach their peak in March. Furthermore, Chuang *et al.* (2013) performed chemical analysis of aerosol samples and suggested that biomass-burning aerosols originated from smoldering softwood. Moreover, northern Indochina features a complex topography and has a high prevalence of forest-conversion fires (i.e., deliberate man-made fires), whereas southern Indochina has a high prevalence of agricultural crop burning. In addition, a larger amount of biomass is burned from forests in northern Indochina compared with the south (Streets *et al.*, 2003).

Ground-based remote sensing instruments (i.e., Sun-sky photometers and lidar) are powerful tools for quantifying smoke haze in terms of aerosol optical properties. Data provided by the well-known Aerosol Robotic Network (AERONET, Holben *et al.*, 1998) are widely used in aerosol research. Using AERONET data, Eck *et al.* (1999) showed that size distributions of biomass-burning aerosols are composed of fine smoke particles. Dubovik *et al.* (2002) compared different fire regions and suggested that Boreal and Amazonian forest fire smoke are less absorbing than grassland-dominated smoke from the African savanna and South American cerrado. Furthermore, recent studies have investigated aerosol mixtures (Eck *et al.*, 2010), types (Giles *et al.*, 2012; Kumar *et al.*, 2014; Sharma *et al.*, 2014), and hygroscopicity (Zhang *et al.*, 2015) associated with haze particles by using AERONET data sets. For determining the vertical profile of smoke aerosols, lidar has proven to be a highly effective tool in aerosol characterization experiments. For example, Welton *et al.* (2002) and Campbell *et al.* (2003) studied biomass-burning aerosols emitted from African savanna fires by using data from the Micropulse Lidar Network (MPLNET). Regarding recent investigations of smoke particles in Southeast Asia conducted using lidar, the long-range transport of Indochinese biomass-burning aerosols over the Dongsha island and Singapore was characterized (i.e., Chew *et al.*, 2013; Wang *et al.*, 2013) during the 7-SEAS experiments.

The 7-SEAS/BASELInE (Biomass-burning Aerosols & Stratocumulus Environment: Lifecycles & Interactions Experiment) was conducted in spring 2013–2015 over northern Southeast Asia to further explore numerous key atmospheric processes and impacts of biomass burning on surface-atmosphere energy budgets during the lifecycles of biomass-burning emissions (Lin *et al.*, 2013). In the current study, we used AERONET and MPLNET data sets obtained from northern Indochina to characterize the aerosol optical properties (i.e., loading, absorption, size, types, and profiles) for in or near-source regions of biomass burning. Brief descriptions of deployments conducted and data used in the analysis are presented in Section 2. The analyses of the spatiotemporal distribution, vertical distribution, diurnal pattern, and optical properties of smoke particles are examined in Section 3, and finally a summary is presented in Section 4.

SITE DESCRIPTION, MEASUREMENTS, AND DATA

Site Description

Fig. 1 shows the AERONET sites used in this study. In addition to original AERONET sites (i.e., Chiang Mai, Mukdahan, Dongsha, and Lulin), we deployed four temporary sites (i.e., Doi Ang Khang, Maesoon, Luang Namtha, and Son La; Table 1) in supporting the 7-SEAS/BASELInE. Doi Ang Khang station (Northern Thailand) is located at the metrological station, Fang District, Chiang Mai Province. It is in a mountain range along the Thai-Myanmar border with an elevation of 1536 m above sea level (a.s.l). In addition to Sun-sky radiometers, a lidar system was deployed to this site during the experiment period. Because this site is surrounded by a forest and converted farmland, smoke emitted from agricultural burning and forest fires have occasionally been observed near the site. Maesoon subdistrict is located at the foothills of Doi Ang Khang. Maesoon station (502 m a.s.l) is set at the office of the Subdistrict Administrative Organization, which is located near a main road. Pollutants from transportation might affect this site. Luang Namtha (northern Laos; 557 m a.s.l) and Son La (northern Vietnam; 683 m a.s.l) are situated in a valley surrounded by mountains. The population of Son La is approximately 20,000, suggesting the site may receive considerable local pollutants. The four sites are in mountainous regions, and the degree of their influence on mountain–valley breeze depends on their geographic locations.

Those four sites are in a region that constitutes a major source of biomass burning emissions over the Indochina peninsula. Fig. 2(a) illustrates Moderate Resolution Imaging Spectroradiometer (MODIS)-derived fire counts obtained from an MCD14ML data set distributed by the NASA Fire Information for Resource Management System. The values represent the sum of fire counts within a $0.5° \times 0.5°$ grid for an intense fire period ranging from March 1 to April 15, 2014. We observed that the fire spots were highly prevalent in mountainous regions with elevations between 0.5 and 1 km. Fire activities were prevalent in eastern Myanmar, at the Thai–Myanmar border, and northern Laos. Note that the underrepresentation of fire counts in Northern Vietnam is due to cloudy environment (Fig. 2(b)). According to the mean wind field of 925 hPa for the same period, the observed sites were located a short distance downwind from the fire spots and were strongly affected by smoke pollutants.

AERONET Direct-Sun and Inversion Data

AERONET deployed CIMEL Electronique CE-318 Sun-sky radiometers to measure the spectral direct-beam solar radiation as well as directional diffuse radiation along

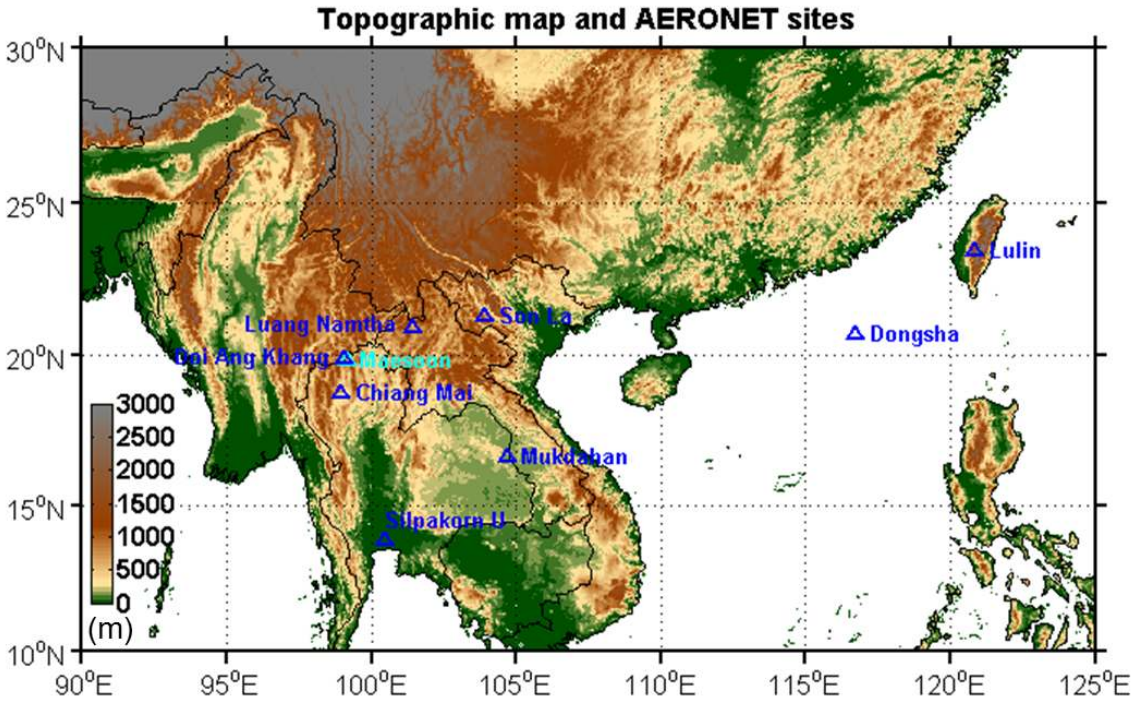

Fig. 1. Topographic map with the location of AERONET sites in the study domain.

the solar almucantar. The direct-beam solar radiation measurements (i.e., direct-sun measurement) were used to determine the columnar aerosol optical depth (AOD or τ) in eight spectral channels (340–1020 nm) with a temporal resolution of approximately 15 min (Holben *et al.*, 1998). The uncertainty of the measured AODs, attributed primarily to the calibration uncertainty, is 0.01–0.02 with the largest uncertainty in the UV (Eck *et al.*, 1999). In this paper, the spectral AOD represented by τ_λ or AOD_λ, where λ is the wavelength in nanometers (nm) and is used to indicate a spectrally varying quantity. The Ångström exponent (AE or α) is another derived quantity, and it is typically used to describe the spectral dependence of the AODs; it is given approximately by $\alpha = -d\ln\tau_\lambda/d\ln\lambda$ over a specified wavelength range. The AE is commonly used to provide basic information on the aerosol size distribution. When sufficient information on the spectral AOD and α is available, the fine (submicron; radius approximately < 1 μm) and coarse (supermicron; radius approximately > 1 μm) AODs at a standard wavelength of 500 nm can be distinguished using the AERONET spectral deconvolution algorithm (O'Neill *et al.*, 2003). The fine mode fraction of AOD (FMF or η) is defined as the ratio of the fine mode AOD to the total AOD at a wavelength of 500 nm. In addition to aerosol properties, the total column precipitable water (PW) in centimeters (cm) can be obtained at a nominal wavelength of 940 nm. These data are cloud screened and quality assured based on Smirnov *et al.* (2000).

In addition to measuring direct solar irradiance, the Sun-sky radiometer measures the sky radiance at four wavelengths (440, 675, 870, and 1020 nm) along the solar almucantar (i.e., at a constant solar zenith angle, with varied azimuth angles). The solar zenith angles are restricted to > 50° (i.e., in early morning and late afternoon). The sky radiance measurements are used to retrieve additional columnar aerosol properties including the volume size distribution, phase function, real and imaginary components of the refractive index, particle effective radius (r_{eff}), single-scattering albedo (ω), and the asymmetry factor (g), which are typically computed using AERONET inversion algorithms (Dubovik and King, 2000; Dubovik *et al.*, 2006; Holben *et al.*, 2006). The uncertainty in the retrieved ω is estimated to be ± 0.03. The absorption AOD or τ_{abs} for a specific wavelength is calculated as follows: $\tau_{abs} = \tau \times (1 - \omega)$. Similar to α, the wavelength dependency of aerosol absorption is typically quantified using the absorption Ångström exponent (AAE or α_{abs}), expressed as $\alpha_{abs} = -d\ln\tau_{abs(\lambda)}/\ln\lambda$. In addition, for absorption-related inversion products (e.g., ω, τ_{abs}, and α_{abs}), the direct-sun Level 2.0 AOD_{440} must be greater than 0.4. AERONET inversion products are quality assured based on Dubovik *et al.* (2000) and Holben *et al.* (2006). In the current study, only AERONET Version 2 Level 2 direct-sun and inversion products were analyzed.

Micropulse Lidar Observations

The NASA MPLNET project is a federated network of ground-based micropulse lidar (MPL) instruments, with continuously operating sites worldwide from the tropics to midlatitudes and the Arctic and Antarctic regions (Welton *et al.*, 2002). The original MPL (Spinhirne *et al.*, 1995) is a compact and eye-safe single polarization elastic backscatter lidar system capable of supporting long-term measurements with a 1-min temporal resolution and 0.075-km vertical resolution. It operates at 527 nm, and the laser pulse duration is approximately 10 ns with a pulse repletion rate of 2500 Hz and output energies in the range of 4–8 μJ $pulse^{-1}$. Campbell *et al.* (2002) and Welton *et al.* (2002) described in detail the

Table 1. Average and standard deviation of aerosol optical properties obtained from four AERONET sites over northern Indochina for period of March 1 and April 15 in 2014. r_{eff_F} and r_{eff_C} present effective radius for fine and coarse mode particles.

Site information	Direct-sun data set					Inversion data set					
	N	τ_{500}	$\alpha_{440\text{-}870}$	PW	η_{500}	N	ω_{440}	$\alpha_{abs440\text{-}870}$	g_{440}	r_{eff_F} (μm)	r_{eff_C} (μm)
Doi Ang Khang (19.93°N, 99.05°E; 1536 m)	2631	0.75 ± 0.41	1.73 ± 0.13	1.23 ± 0.31	0.95 ± 0.03	71	0.89 ± 0.02	1.48 ± 0.25	0.67 ± 0.02	0.14 ± 0.01	2.36 ± 0.42
Maesoon (19.83°N, 99.17°E; 502 m)	1054	1.37 ± 0.65	1.75 ± 0.12	2.24 ± 0.52	0.96 ± 0.02	102	0.86 ± 0.02	1.49 ± 0.14	0.67 ± 0.02	0.14 ± 0.01	2.51 ± 0.39
Luang Namtha (20.93°N, 101.42°E; 557 m)	2635	1.25 ± 0.58	1.73 ± 0.11	2.58 ± 0.63	0.96 ± 0.02	38	0.86 ± 0.03	1.57 ± 0.23	0.68 ± 0.02	0.14 ± 0.01	2.52 ± 0.37
Son La (21.33°N, 103.91°E; 683 m)	1652	1.49 ± 0.60	1.69 ± 0.10	2.57 ± 0.45	0.97 ± 0.02	35	0.89 ± 0.02	1.46 ± 0.26	0.69 ± 0.03	0.16 ± 0.01	2.59 ± 0.37

standard instrument design and Level 1 signal processing. In the current study, a new MPL system (532 nm) was deployed in the field for the first time. The system was manufactured by Sigma Space Corporation, United States, but with modifications enabling polarization-sensitive measurements for autonomous analysis of aerosol and clouds.

In the current study, MPLNET Version 2 Level 1.5 data sets were used. The Level 1.5 aerosol properties were derived using an algorithm proposed by Welton *et al.* (2000); in this algorithm, the AERONET AOD is used as the constraint to solve the lidar ratio and the aerosol extinction profile from the cloud-screened 20-min signal averages. A daytime mean lidar ratio was applied to the calculation of the nighttime extinction profile for a single day because AERONET data were not available at night. The mean uncertainty in the MPLNET-retrieved extinction is ± 0.015 km^{-1}.

RESULTS AND DISCUSSION

Spatiotemporal Variability in AOD

Biomass-burning aerosols are the predominant type of aerosol over Indochina during the spring months. Previous studies (e.g., Gautam *et al.*, 2012; Lin *et al.*, 2014) have demonstrated the aerosol inter-annual variability of aerosol loading over the Indochina peninsula based on MODIS monthly AOD. Furthermore, Yen *et al.* (2013) and Tsay *et al.* (2013) suggested that the inter-annual variability is highly correlated with precipitation and large-scale climate variability. In the current study, we conducted a climatological assessment for seasonal AOD variation based on AERONET data. Five AERONET sites (i.e., Chiang Mai Met Station, Silpakorn University, Mukdahan, Dongsha Island, and Lulin), located in or downwind of Indochinese biomass-burning aerosol source regions, were evaluated. In this paper, the discussion is focused on the peak AOD in spring induced by biomass-burning smoke aerosols. As shown in Fig. 3, all AERONET sites in the region show seasonal high AODs in March, indicating the regional impact of Indochinese smoke haze. The spatial distribution and transport of smoke haze are complicated because of the complex terrain (Fig. 1), emission intensity (Fig. 2(a)), and different flow patterns in height (low-level updraft and convergent flow and upper-level westerlies; see Lin *et al.*, 2013 for details) in the study domain.

Traditionally, the Chiang Mai Met Station represents to a site with strong influences by biomass burning (mean AOD approximately 0.5 in March) in northern Thailand, despite the biomass burning aerosols being composed of urban and industrial aerosols (Gautam *et al.*, 2012). Compared with the AOD in February, three sites (i.e., Chiang Mai Met Station, Dongsha, and Lulin) demonstrated significant increases of more than double in the AOD, suggesting their high potential for Indochinese smoke monitoring. The transport of Indochinese smoke aerosols over Lulin and Dongsha has been thoroughly studied (i.e., Lin *et al.*, 2013; Wang *et al.*, 2013 and the references therein). By contrast, two sites (i.e., Silpakorn University and Mukdahan) in southern Thailand showed only slight increases in the AOD during the peak biomass-burning season, implying that a mixture of various aerosols may contribute to their aerosol loading.

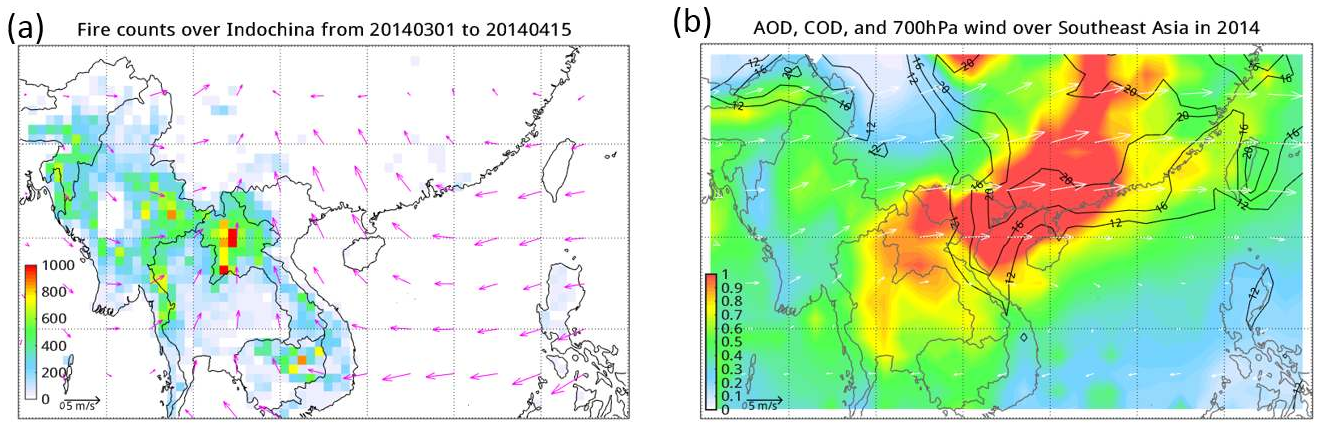

Fig. 2. Maps of (a) 0.5° × 0.5° gridded total fire counts , and (b) 1° × 1° aerosol optical depth (shaded) and cloud optical depth (contour) at wavelength 550 nm obtained from the MODIS instrument aboard the Terra satellite during March 1 and April 15 2014 . The 1° × 1° NCEP reanalysis 925 hPa and 700 hPa winds (vector) are also shown in the figure.

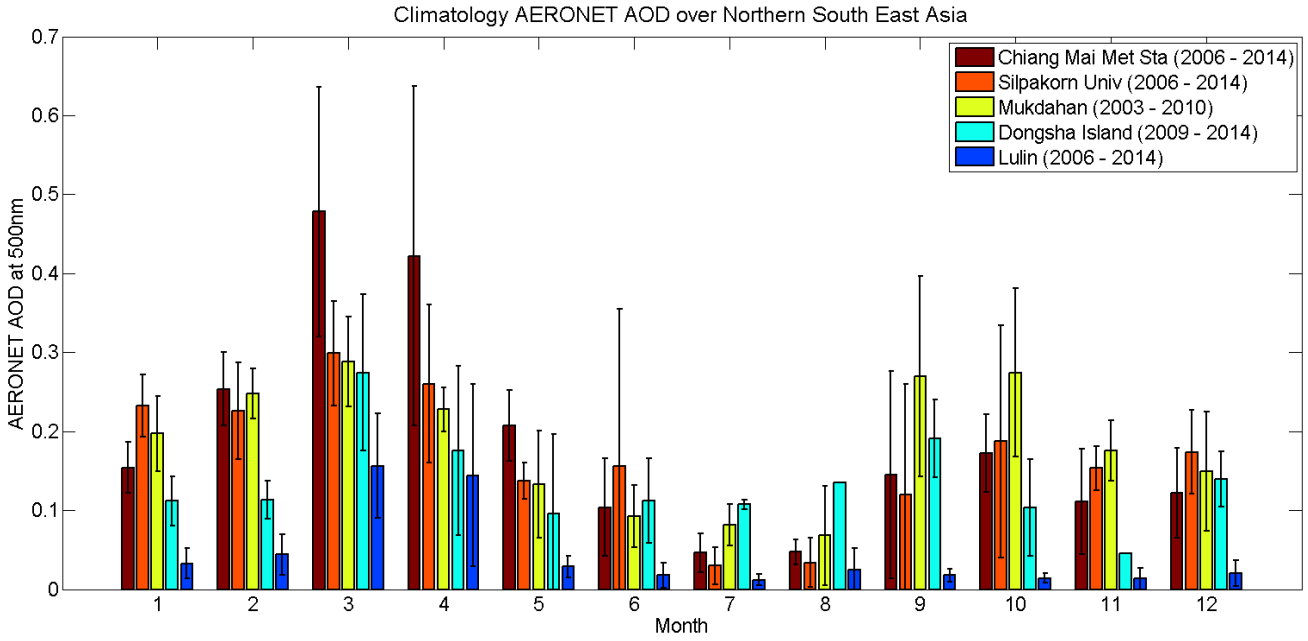

Fig. 3. Monthly variation of AOD at the five selected AERONET sites in the northern Southeast Asia. The data was downloaded form AERONET climateology data page (Holben *et al.*, 2001) and data period used for statistics are shown in the parentheses of legend.

In this study, daily MODIS-terra Level 3 data (MOD08) obtained from the Giovanni online data system (http://disc.sci.gsfc.nasa.gov/giovanni/) were used to characterize the spatial distribution of smoke plumes. Fig. 2(b) shows the composite mean AOD and cloud optical depth (COD) at a 1° × 1° resolution for the study period ranging from March 1 to April 15, 2014. Furthermore, 700 hPa wind data obtained from National Centers for Environmental Prediction reanalysis data set (http://www.esrl.noaa.gov/psd/data/gridded/data.ncep.reanalysis.html) are plotted in this figure. The high AOD in northern Vietnam and southern China consistently overlaps considerably with the high COD (> 12) area, indicating possible cloud contamination in satellite-retrieved AODs over cloudy environments (e.g., Huang *et al.*, 2011) and an implication for aerosol and cloud interactions (e.g., Lee *et al.*, 2014; Lin *et al.*, 2014). In the cloud-free region of the Indochina peninsula, high AODs (> 0.8) were observed over northern Thailand, Laos, and Vietnam. The high AOD over northern Indochina is due to the intense fire activities and the accumulation of aerosols because of the southerly convergent flows at the surface and the terrain blockage in the north.

Fig. 4 illustrates the daily variation in the AODs measured at the four AERONET sites during the experimental period in 2014. The daily mean AODs for Doi Ang Khang, Maesoon, Luang Namtha, and Son La were 0.75, 1.36, 1.24, and 1.46, respectively. The large difference in the mean AOD among the four sites indicates the inhomogeneity of aerosol loading in response to site elevations and air mass sources. The low AOD observed in Doi Ang Khang is attributable

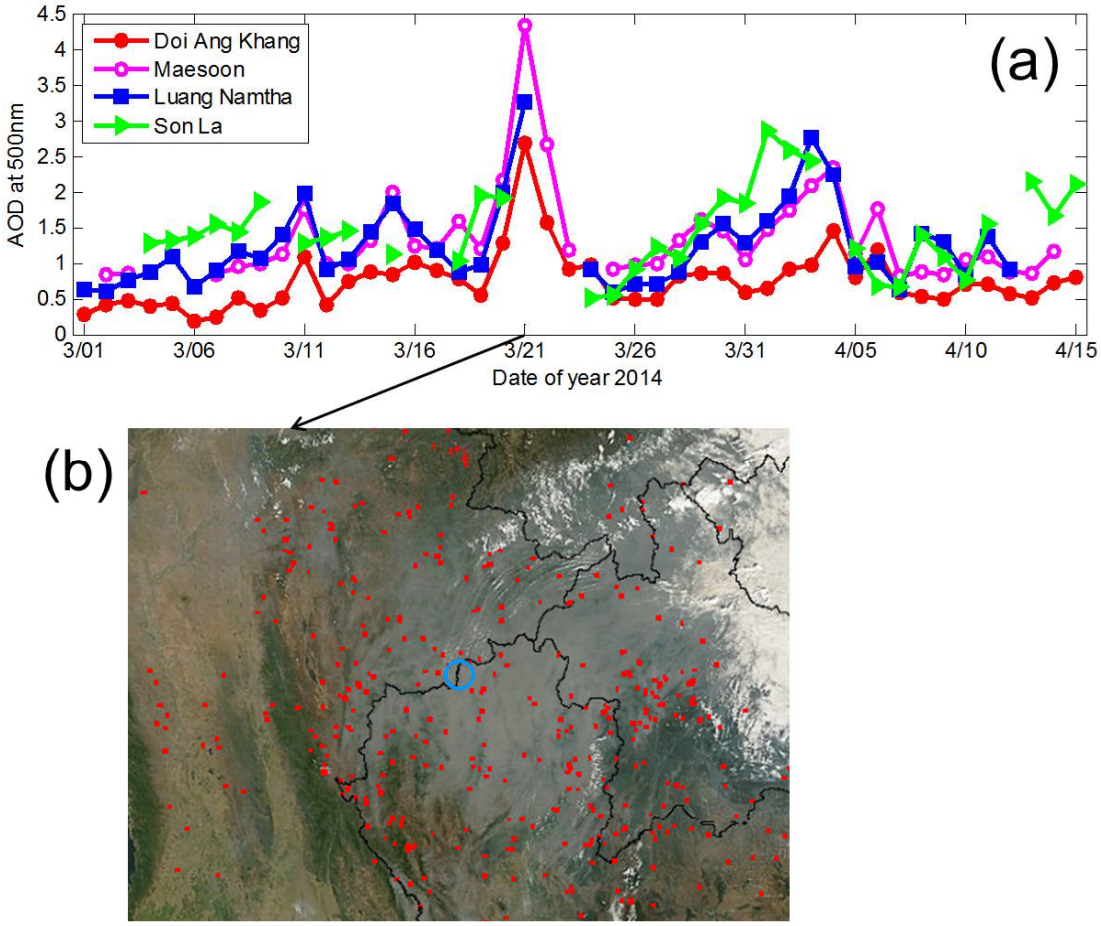

Fig. 4. (a)Time series of daily AOD_{500} at four AERONET sites over northern Indochina from March 1 to April 15, 2014. (b) Terra MODIS rapid response image centered on Doi Ang Khang at ~04:00 UTC on 21 March 2014. The image shows detected fires (in red), smoke (light gray), and clouds (white) in northern Indochina. The image was obtained from the Land, Atmosphere Near real-time Capability for EOS (LANCE) web site (https://earthdata.nasa.gov/data/near-real-time-data/rapid-response).

to the site's relatively high elevation. By contrast, the other three valley sites with similar elevation (approximately 600 m a.s.l) demonstrated considerably higher AODs compared with that at the hilltop site. Comparing the AOD trends for the four sites, the time evolution of the AOD exhibited highly consistent temporal distribution patterns, implying a widespread haze smoke over the region (Fig. 4(b)). The major variability caused by changes in the magnitude of the AOD is mediated by meteorological conditions. For example, a thick smoke condition (AOD up to 4.3) was observed on March 21, 2014. Decreasing mixed layer height (as determined by lidar observation) and stable synoptic conditions (i.e., high pressure and weak wind speed) on 21 March combined with intense forest fires, leading to stagnant air masses, may be the main reason for the severity of the haze episode.

Vertical Distribution of Smoke Aerosol

We studied the aerosol vertical distribution over northern Thailand by using MPL aerosol extinction profiles. To demonstrate the aerosol evolution in temporal and vertical scales, we selected a 6-day period (Fig. 5(a)). The time series of the aerosol extinction profile exhibited a diurnal cycle associated with PBL development. A shallow mixed layer with a height of approximately 1 km occurred in the morning, and this height increased with the solar radiation intensity. When thermal heating and mountain breeze agitated the mixed layer, its maximum height reached 3 km around 16:00 local time. Higher aerosol extinctions were observed in the top of the mixed layer on March 9, 10, and 11. According to HYSPLIT back trajectory and MODIS fire count analysis (Fig. 5(b)), the upper layer of the aerosol distribution originated from forest fires in southeast of Doi Ang Khang in the morning or on the previous day. During this period, we also observed some high aerosol extinction values near the ground (i.e., March 10), suggesting fire activities close to the site, which is consistent with *in situ* measurement results (not shown). In Fig. 4, the daily AOD showed a slow buildup of haze air masses. The accumulation process of aerosol particles occurred successively from Day 1 to Day 5, and dissipation of smoke occurred on Day 6. This suggests that the synoptic scale meteorology (i.e., rainfall episodes) may influence in the temporal evolution of the regional air quality and its explanation requires further investigation in a separate study.

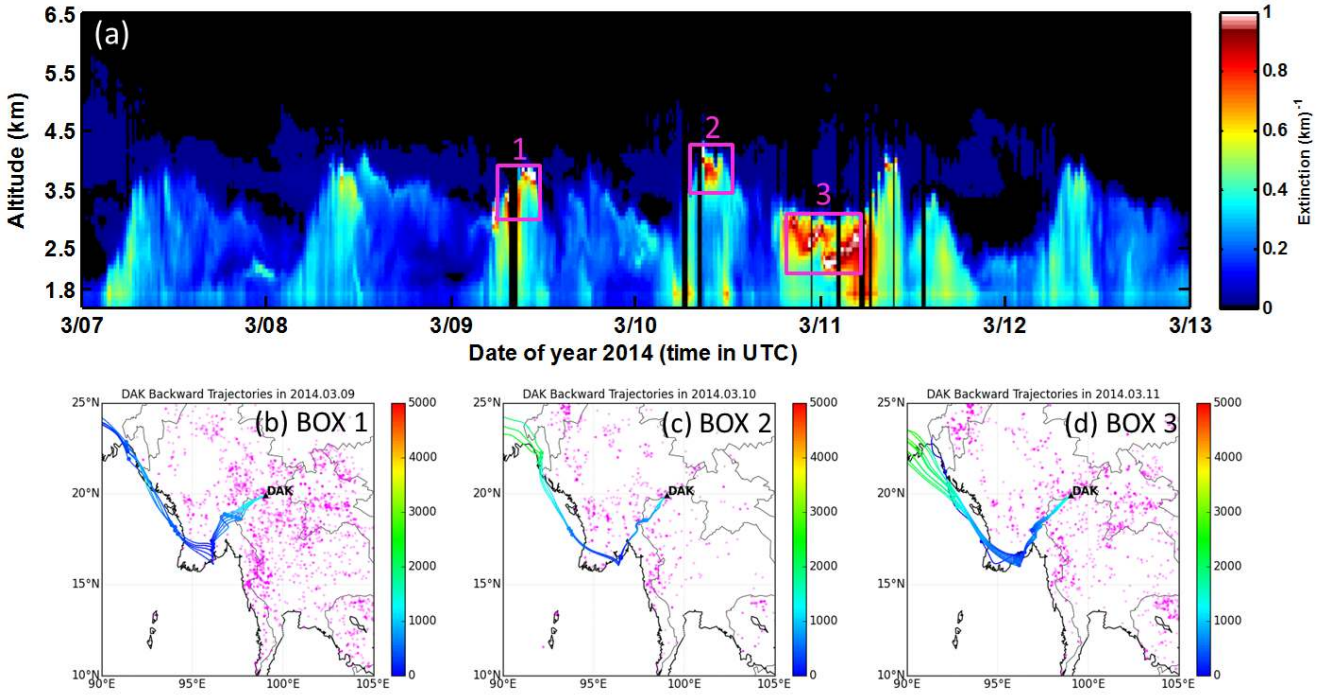

Fig. 5. (a) time series of aerosol extinction profiles at Doi Ang Khang from March 7 to March 12, 2014. The three boxes represent high aerosol plumes during the period. (b)-(d) HYSPLIT backward trajectories and daily MODIS fire counts corresponding to the three boxes. The methodology of five-day backward trajectory can be referred to Wang *et al*. (2013). Trajectory altitudes (based on the mean sea level, in meters) are denoted by the color scale. The daily fire counts data was obtained from the 7-SEAS Data Repository (http://www.nrlmry.navy.mil/aerosol_web/7seas/7seas.html).

Regarding the mean aerosol extinction profile for the entire period (Fig. 6(a)), we observed that the peak of the mean aerosol extinction near the surface was 0.3 km^{-1}, and the aerosol height reached 5 km a.s.l. A high standard deviation associated with diurnal variability was observed in the data set. We also assessed the 3-h mean aerosol extinction profile (Fig. 6(b)). In general, aerosol profiles changed significantly due to PBL development considered as the primary factor; however, diurnal fire emission pattern and transport of smoke aerosols from neighboring areas can have contributions to the magnitude of aerosol loading in different vertical layers. The morning profile (observed at 7:00–10:00 local time) showed the lowest aerosol extinction. As the biomass-burning emission intensified throughout the daytime, the aerosol loading increased and peaked in the evening (16:00–19:00). At 13:00–16:00, the surface temperature peaked, leading to the formation of an adequately mixed smoke layer extending from the surface to a height of 2.5 km (~4 km a.s.l). At 16:00–19:00, we observed a two-layer structure of aerosol distribution. The upper layer may have been caused by the accumulation of aerosols near the boundary of temperature inversion layer (Nodze *et al.*, 2006) and transport of smoke/dust aerosols from upwind areas (i.e., southeast Myanmar) (Gautam *et al.*, 2012; Alam *et al.*, 2014). Because of atmospheric cooling at night, the descent of the mixing layer constrained smoke aerosol to lower levels, leaving the nocturnal mixing layer above it (Fig. 5(a)). Throughout the nighttime, the aerosol loading exhibited successive declines, suggesting the concentration of smoke aerosol was diluted by stronger westerly winds at night (3 m s^{-1} vs. 1.3 m s^{-1} in the morning) and dispersed to downwind areas.

We compared satellite lidar (Gautam *et al.*, 2012) results with the MPL results derived in the current study; we determined that both results are highly consistent regarding the vertical structure of aerosols, implying that space-borne lidar is an effective instrument for obtaining regional aerosol pollution in vertical profiles. However, Gautam *et al.* (2012) reported only the nighttime aerosol profile because high data quality is obtained at nighttime; therefore, the mechanism of strong aerosol diurnal variability over the region is not resolved. The results of the current study exhibit an aerosol profile with a higher temporal resolution covering both the daytime and nighttime, indicating the presence of aerosols reaching approximately 5 km a.s.l., which is higher than the value (approximately 4 km a.s.l) suggested by Gautam *et al.* (2012). When smoke aerosols move to higher altitudes, they have a high potential for long-range transport by westerly winds and for being transported to downwind areas, such as Son La and the West Pacific (e.g., Lin *et al.*, 2013). Regarding the quantity of aerosol extinction, a higher value was observed for MPL compared with that reported by Gautam *et al.* (2012) (0.27 km^{-1} vs. 0.16 km^{-1} at an elevation of 2 km a.s.l). The discrepancy is associated with a data-sampling problem as well as the statistical methods applied to the data sets. A more detailed comparison such as evaluating each satellite lidar profile by using MPL should be an appealing topic for future study.

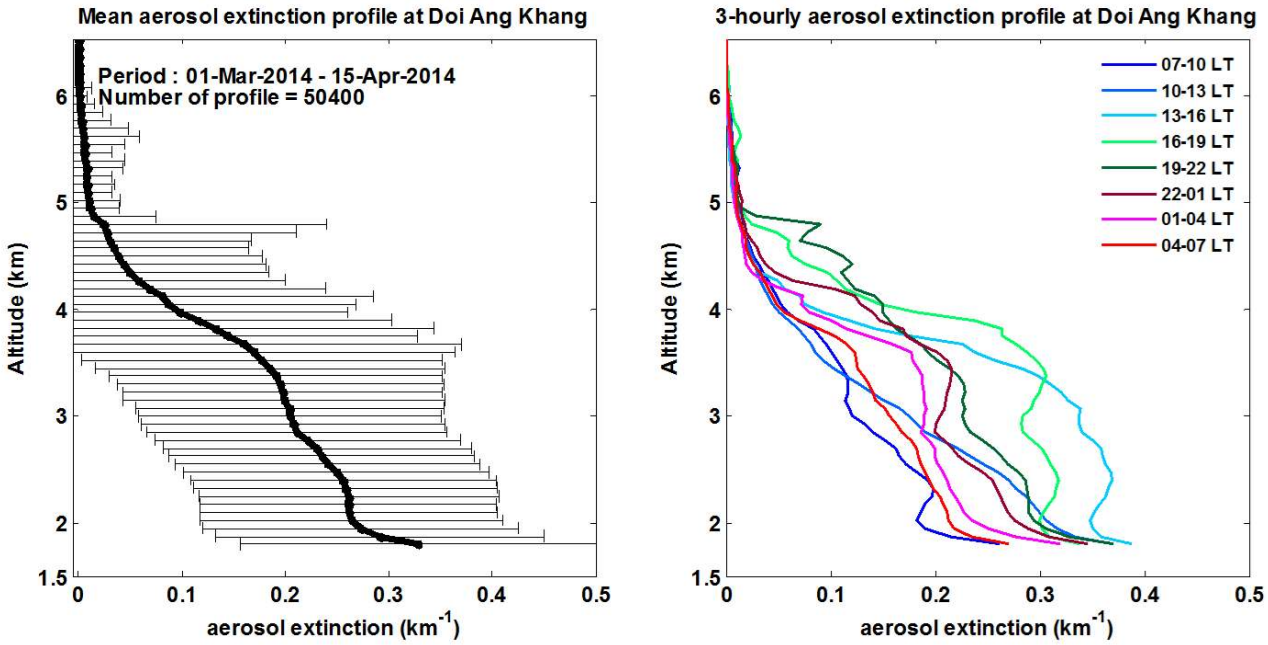

Fig. 6. (a) mean aerosol extinction profile with stand deviation and (b) mean 3-hr aerosol extinction profiles in local time during March 1 and April 15, 2014.

Diurnal Variability of Aerosol Optical Properties

We investigated the daytime variability of smoke aerosols over northern Indochina. Fig. 7 shows the mean hourly AOD_{500}, $AE_{440/870}$, and PW patterns for the four AERONET sites. The mean hourly values were calculated from the AERONET direct-sun measurement data set for March 1 and April 15 in 2014. A pronounced daytime pattern was observed at Doi Ang Khang; this pattern demonstrated a relatively low aerosol loading throughout the morning followed by a gradual and steady increase from the forenoon through the afternoon and then a peak AOD at approximately 15:00–16:00. This pattern is highly consistent with the integrated aerosol loading observed in the 3-h mean aerosol extinction profile obtained using the lidar observation (Fig. 6(b)), confirming that the high AOD in the afternoon is induced by the increased concentration of smoke aerosols at the upper level. The peak AOD exhibited a strong correlation with the high AE (up to 1.85), indicating that aerosols with small particles dominated the increase in AOD. The aerosol particles rose to the station elevation, where the content of water vapor was considerably lower than measured in the valley location. We suggest that the possibility that water in the aerosol particles evaporates when the aerosol particles are rising, leading to the existence of finer smoke particles. Furthermore, Reid *et al.* (1998) reported that in Brazil, the AE value of fresh smoke particles was 2.5 and that of well-aged smoke particles was 0.5. Therefore, fine aerosol particles may be observed in the afternoon at Doi Ang Khang because smoke contained relatively fresh particles contributed by nearby fires.

To explore the difference in the diurnal AOD_{500} patterns between the hilltop (i.e., Doi Ang Khang; 1536 m a.s.l) and valley sites, we conducted an experiment by deploying an AERONET radiometer at Maesoon (502 m a.s.l) in 2014. The hourly AOD trend for Maesoon was similar to that for Doi Ang Khang, except for the morning hours. The high AOD in the morning is a typical feature for the three valley sites and is related to the smoke aerosol confined within the PBL; however, this feature was not observed in Doi Ang Khang because it is positioned above PBL in the morning. The mean AOD_{500} of Measoon was 1.8 times higher than that of Doi Ang Khang (Table 1). The differences between the two sites were 0.61 for AOD and 1.0 cm for PW, suggesting that the shallow and thin atmospheric layer (thickness of approximately 1 km) contains a large amount of smoke aerosols and water vapor. For the 1-km-thick layer, the mean aerosol extinction was approximately 0.61 km^{-1}, which is double that retrieved using the MPL (approximately 0.3 km^{-1}) at Doi Ang Khang. The aerosol extinction observed by Gautam *et al.* (2012) was not as high as those observed in the current study (i.e., between 0.5 and 1.5 km a.s.l) because they calculated a long-term regional average. We suggest that a thick aerosol layer at the valley may have considerable effects on the atmospheric radiation budget and must be explored in the future. Moreover, the two sites showed a greater difference in the AE values in the morning; by contrast, they showed consistent AE values in the afternoon. The higher AE values of Maesoon in the morning are most likely caused by the contribution of fresh aerosols from biomass burning. In the afternoon, PBL processes provided an efficient mechanism to mix aerosols within the layer to promote the existence of mainly fine mode aerosols.

In this paper, we summarized the daytime AOD patterns for the three valley sites. An initial AOD value was determined according to the aerosol loading before sunrise. The increase in the AOD during the morning hours was strongly related to man-made fire activities, which continued until noon when farmers took a break. Meanwhile, the

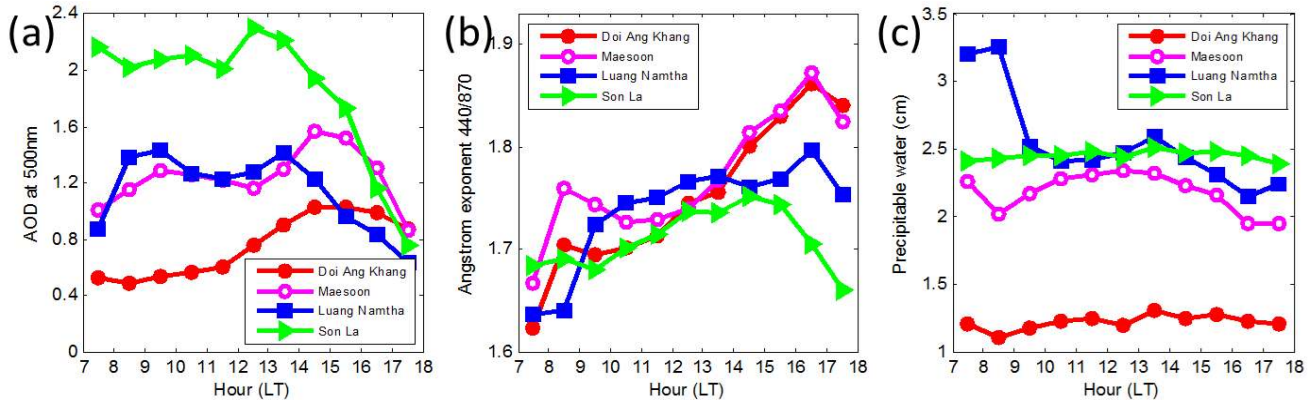

Fig. 7. Daytime diurnal variability of (a) AOD at 500 nm, (b) Angstrom exponent (440–870 nm) and (c) precipitable water in cm obtained from four AERONET sites from March 1 to April 15, 2014.

expansion of aerosol mixed layer height induced by solar heating enabled smoke aerosols to rise to higher levels. The aerosol loading increased with the PBL height and peaked at approximately 14:00. The AOD peak time may be delayed if transported smoke aerosols arrive at the site (Fig. 7(a), Maesoon). The significant decline in the AOD after 14:00 suggests the dispersion of upper-level smoke plumes by stronger westerly winds as well as the descent of the PBL height. Among the typical diurnal patterns, we observed a distinct AOD pattern for Son La during morning hours. We conducted a trajectory analysis (not shown) and determined that the high AOD in the morning may be due to the contribution of aerosols transported from eastern Vietnam, which involved biomass-burning and anthropogenic emission sources. The highest mean AOD was observed at Son La because of the diversity of emission sources including biomass burning, urban, industrial, and transportation.

Assuming a nearly constant aerosol composition, the aerosol size can change with the relative humidity of the environment, which is the so-called aerosol hygroscopic growth. As depicted in Fig. 7(c), in the dry season in northern Indochina, the measured PW remained lower and nearly constant (approximately 2.2–2.6 cm) compared with that measured in the wet season (approximately 5 cm) at Chiang Mai Met Station. The PW measured between 08:00 and 09:00 and 16:00 and 17:00 for several sites was lower when the AE value increased. For the two short periods, we determined that more fresh aerosols may be emitted from transport and biomass-burning activities. Abundant fresh aerosols can absorb water vapor from the air, possibly leading to a decline in the PW. For Luang Namtha, a higher PW was observed in the early morning. We believe that the higher water vapor is related to the local climate condition because the site is located in the southern foot of high mountains. The lower AE corresponding to the high PW in the morning suggests that haze particles experienced hygroscopic growth from the night to the early morning. By contrast, the PW values remained constant for the Son La site despite the significant reduction in the AE values in the afternoon hours. This may be attributed to the change in aerosol compositions (i.e., invasion of local and urban/industrial pollutants) in the air mass.

Aerosol Optical Properties

In this section, the optical properties of biomass-burning aerosols over northern Indochina are presented and compared with those of aerosols from worldwide biomass-burning regions. Table 1 shows the statistics of the aerosol optical properties from the four AERONET sites in northern Indochina from March 1 to April 15, 2014. Key parameters from direct-sun and inversion data sets with diverse sampling numbers are listed in the table.

The general characteristics of the biomass-burning aerosols over northern Indochina are described according to the four AERONET sites. The aerosols are predominantly composed of fine mode particles ($\alpha_{440\text{-}870}$ of 1.72, η of 0.96) with strong absorption (ω_{440} of 0.88). The mean columnar aerosol loading (τ_{500}) and water vapor (PW) over the region are 1.22 and 2.16 cm, respectively, suggesting a heavy hazy environment during the dry season. However, the sites demonstrated slightly different columnar aerosol loading and water vapor values because of their geographical locations and local meteorological conditions. For example, the lowest AOD (0.77) and PW (1.27 cm) were observed at Doi Ang Khang because of its higher elevation. Aerosol optical properties of Son La (highest AOD, FMF, SSA, r_{eff}, and lowest $\alpha_{440\text{-}870}$, $\alpha_{abs440\text{-}870}$) were different from those of the other sites. As discussed, these dissimilarities were caused by diverse emission sources (i.e., biomass-burning and urban/industrial aerosols). In general, the optical properties of smoke haze measured at Doi Ang Khang were closest to the source region and had minimal effects from anthropogenic aerosols. Maesoon and Luang Namtha represented aerosol characteristics in the valley region, encompassing northern Thailand and Laos. Smoke haze over the valley region contains highly absorbing aerosols (ω_{440} of approximately 0.86). For Son La, the measurement results represented aerosol characteristics over the northeast Indochina peninsula, suggesting a mixture of biomass-burning and anthropogenic aerosols. Therefore, the dynamic properties of the aerosol environment over northern Indochina were determined according to the spatial distribution of aerosol optical properties, which were strongly influenced by local factors (e.g., PBL dynamics, local meteorology, and emission sectors).

AERONET observations of aerosols with ω_{500} greater than 0.95 are considered low absorbing aerosols, whereas ω_{500} less than 0.88 are considered strong absorbing aerosols. For tropical fires, a lower value of ω_{500} (approximately 0.85) indicates fresh aerosol from biomass burning, and when the value increases considerably (up to approximately 0.90) within 2 h, the aerosol is considered aged aerosol (e.g., Abel *et al.*, 2003). Furthermore, black carbon (BC) particles have the strongest absorption in the near-infrared region of the electromagnetic spectrum, whereas aerosols composed of brown carbon (BrC) or organic carbon (OC) exhibit stronger absorption in the ultraviolet and visible bands (Eck *et al.*, 2009). The parameter g is the fraction of the incident radiation scattered forward after striking an aerosol. The value of g is equal to 1 if 100% of the incident radiation is scattered forward, whereas the value of g is equal to 0 if one half of the incident radiation is forward-scattered and the other half is backscattered.

Fig. 8 shows aerosol optical properties (i.e., ω, g, and τ_{abs}) at varying wavelengths at the four AERONET sites. Data in the morning and afternoon hours are separately plotted in the figure. The results showed that the mean ω_{440} value was approximately 0.88 and that ω decreased with the increase in wavelength, suggesting that biomass-burning smoke is an absorbing aerosol with a high concentration of BC produced by combustion. The lowest ω values, particularly for the near-infrared region, were observed at Luang Namtha and Maesoon. This suggests that smoke particles with a higher BC concentration occurred along the Thai-Laos valley. Moreover, the spectral dependence of g at Luang Namtha was lower than that at the other sites. We assumed that the southerly convergent flows transported anthropogenic pollutants from southern Thailand and converged at the two sites (Fig. 2(a)). Anthropogenic pollutants containing absorbing aerosols can enhance the absorption property of aerosols. However, weaker aerosol absorptions (ω_{44} = 0.89) and similar ω spectra were observed at Doi Ang Khang and Son La. The weak absorption property suggests the presence of aged aerosols from tropical fires or urban/industrial aerosols. Giles *et al.* (2012) reported that identifying the aerosol type by using only AERONET data is challenging because of the similarity in the optical properties of biomass-burning and urban/industrial aerosols. Auxiliary data such as backward trajectories, aerosol chemistry, and *in situ* aerosol measurements are useful for further identification, which can be conducted in a separate study. All sites exhibited a pronounced reduction in the g spectrum as λ increased, and this finding is highly consistent with the optical feature of biomass-burning aerosols reported by Dubovik *et al.* (2002). The g spectrum showed a stronger decreasing trend for afternoon hours than for morning hours. Smoke aerosols in the afternoon had weaker forward scattering than they did in the morning, particularly in the near-infrared region, indicating the presence of smaller particles from either fresh or transported aerosols.

Table 2 shows a comparison of the optical properties of aerosols from worldwide major biomass-burning regions. According to Giles *et al.* (2012), the aerosol types can be inferred from AERONET data sets by carefully separating the aerosol particles according to their absorption properties (i.e., ω and α_{abs}) and size (i.e., α_{ext} and η). As shown in Table 2, the ω_{440} values for biomass burning aerosols varied significantly (ranging from 0.85 to 0.95) for smoke originating from distinct regions. Aerosols from the African Savanna demonstrated the strongest absorption (generally lowest ω) with the strongest spectral dependence, whereas those from the boreal forest exhibited the weakest absorption. Most of the differences in the absorption magnitude may be attributable to numerous factors such as the flaming versus the smoldering phases, effect of the fuel moisture content, degree of aging of the particles, ambient temperature, relative humidity, and fire intensity (Dubovik *et al.*, 2002

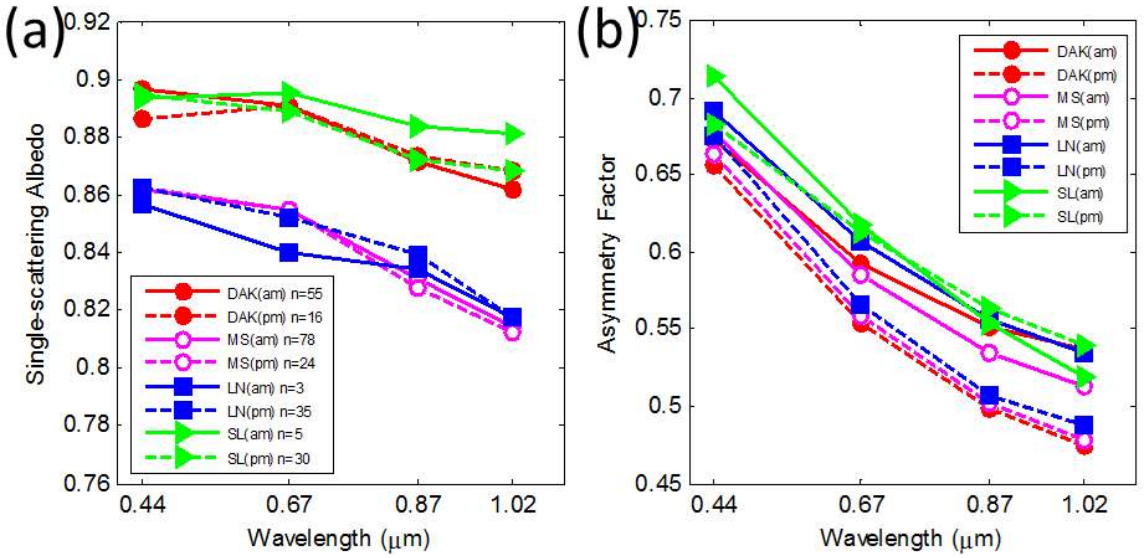

Fig. 8. AERONET retrieval of aerosol optical properties, (a) single-scattering albedo, and (b) asymmetry factor as change with wavelength obtained from four sites over northern Indochina during March 1 and April 15, 2014. Solid line and dash lines denote spectral dependence of SSA and asymmetry factor in the morning and afternoon, respectively.

Table 2. Aerosol optical properties from worldwide biomass-burning source regions.

Region	Fire Type	ω 440/675/870/1020 nm	$\alpha_{abs440\text{-}870}$	$\alpha_{440\text{-}870}$*	η_{500}*	Reference
Northern Indochina	Forest and agricultural	0.88/0.87/0.85/0.84	1.5	1.8	0.95	this study
Amazon	Forest	0.93/0.92/0.90/0.89	1.5	1.9	0.92	Giles *et al.* (2012)
Australia	Forest	0.85/0.83/0.82/0.81	1.4	1.5	0.79	Giles *et al.* (2012)
North America	Boreal Forest	0.95/0.96/0.96/0.95	1.8	1.5	0.96	Giles *et al.* (2012)
Africa	Savanna	0.87/0.83/0.80/0.77	1.2	1.9	0.92	Giles *et al.* (2012)

* calculated from AERONET inversion data set.

and references therein). High BC concentration is typically observed in the flaming phase. African Savanna and northern Australian grasses emit high concentrations of absorbing aerosols which resulting in low ω values. In the current study, the data for the Indochina fire smoke suggested that flaming phase fires likely produced considerable amounts of absorbing aerosols (i.e., BC). Moreover, the mean α_{abs} (i.e., 1.5) was within the range of 1.2–1.8 reported by Giles *et al.* (2012) for biomass burning regions. The α_{abs} value of BC is approximately 1 for very small particles, whereas that of BrC varies from 1.5 to 7 (Hoffer *et al.*, 2006). For α_{ext} and η, the mean values were calculated from the inversion data set and were slightly different from the values shown in Table 1 due to fewer number of almucantar inversions versus solar measurements. Compared with results from Giles *et al.* (2012), the α_{ext} and η values derived in the current study were consistent with those in other regions. Overall, according to the comparison results, we conclude that the biomass-burning aerosols in northern Indochina are distinct from those in other regions. For example, Indochina smoke may be more absorbing (lower SSA values) than Amazon smoke with similar particle size but Indochina smoke may contain less BC (lower AAE values) than in sub-Saharan Africa and northern Australia smoke. This lower SSA has a vital implication for the satellite retrieval of the AOD in applying a local smoke model in retrieval algorithms (More *et al.*, 2013).

SUMMARY

Northern Indochina is a region with a considerable amount of smoke aerosols because of the prevalence of man-made fires. In this study, we evaluated aerosol optical properties and vertical structure of biomass-burning aerosols over northern Indochina by using ground-based remote sensing data obtained from the 7-SEAS/BASELInE in 2014. We deployed one MPLNET lidar and four AERONET Sun-sky radiometers for the first time to characterize aerosol features over a region encompassing northern Thailand, Laos, and Vietnam. The results are summarized as follows:

- Aerosol loading over Indochina exhibits a highly consistent temporal distribution pattern suggesting the presence of widespread smoke haze from ground-based measurements and satellite-based retrievals. The complex terrain and meteorological conditions of the region considerably affects aerosol loading. A higher mean τ_{500} of ~1.4 is observed at Measoon (in the valley), whereas a lower mean τ_{500} of ~0.75 is observed at Doi Ang Khang (hilltop).
- The optical properties of biomass-burning aerosols over northern Indochina indicate abundant fine mode (η_{500} of 0.96 and $\alpha_{440/870}$ of 1.72) mixture of black carbon and brown carbon particles (α_{abs} of 1.5) with strong absorption (ω_{440} of 0.88). Slightly stronger absorption (ω_{440} of 0.86) is observed over the Thai-Laos valley.
- A smoke haze layer is observed and it extends from the surface to 5 km a.s.l with strong diurnal variability. The result shows in good agreement with satellite lidar observation.

- A strong diurnal pattern over northern Indochina is observed in the columnar aerosol optical data. In general, smoke aerosol particles observed in the morning are aged and large, whereas those observed in the afternoon are relatively fresh and small. The diurnal variability is mainly attributable to PBL development, whereas the fire intensity and transported smoke adjust the magnitude of aerosol loading.
- The overall aerosol optical characteristic in northern Indochina is unique and distinct from those in various biomass-burning regions. The results have vital implications for the satellite retrieval of biomass-burning aerosols over northern Indochina.

ACKNOWLEDGEMENTS

This work was supported by the National Science Council of Taiwan under grants No. MOST 103-2111-M-008-006, 101-2119-M-008-012 and by the Taiwan EPA under contracts No. EPA-103-U1L1-02-101. The 7-SEAS, AERONET, MPLNET, project was supported by the NASA Radiation Sciences Program managed by Dr. Hal Maring. The authors thank the AERONET team for calibrating and maintaining instrumentation and processing these data. Thanks are also given to all assistants and graduate students involving in the site operation, data analysis and technical support for making 7-SEAS/BASELInE campaign successful.

REFERENCES

Abel, S.J., Highwood, E.J., Haywood, J.M. and Stringer, M.A. (2005). The Direct Radiative Effect of Biomass Burning Aerosols over Southern Africa. *Atmos. Chem. Phys.* 5: 1999–2018.

Alam, K., us Sahar, N. and Iqbal, Y. (2014). Aerosol Characteristics and Radiative Forcing during Pre-Monsoon and Post-Monsoon Seasons in an Urban Environment. *Aerosol Air Qual. Res.* 14: 99–104.

Campbell, J.R., Hlavka, D.L., Welton, E.J., Flynn, C.J., Turner, D.D., Spinhirne, J.D., Scott, V.S. and Hwang, I.H. (2002). Full-Time, Eye-Safe Cloud and Aerosol Lidar Observation at Atmospheric Radiation Measurement Program Sites: Instruments and Data Processing. *J. Atmos. Oceanic Technol.* 19: 431–442.

Campbell, J.R., Welton, E.J., Spinhirne, J.D., Ji, Q., Tsay, S.C., Piketh, S.J., Barenbrug, M. and Holben, B.N. (2003). Micropulse Lidar Observations of Tropospheric Aerosols over Northeastern South Africa during the ARREX and SAFARI 2000 Dry Season Experiments. *J. Geophys. Res.* 108: 8497.

Campbell, J.R., Reid, J.S., Westphal, D.L., Zhang, J., Tackett, J.L., Chew, B.N., Welton, E.J., Shimizu, A., Sugimoto, N., Aoki, K. and Winker, D.M. (2013). Characterizing the Vertical Profile of Aerosol Particle Extinction and Linear Depolarizat on over Southeast Asia and the Maritime Continent: The 2007–2009 View from CALIOP. *Atmos. Res.* 122: 520–543.

Chew, B.N., Campbell, J.R., Salinas, S.V., Chang, C.W., Reid, J.S., Welton, E.J., Holben, B.N. and Liew, S.C. (2013). Aerosol Particle Vertical Distributions and Optical Properties over Singapore. *Atmos. Environ.* 79: 599–613.

Chuang, M.T., Chou, C.C.K., Sopajaree, K., Lin, N.H., Wang, J.L., Sheu, G.R., Chang, Y.J. and Lee, C.T. (2013). Characterization of Aerosol Chemical Properties from Near-source Biomass Burning in the Northern Indochina during 7-SEAS/Dongsha Experiment. *Atmos. Environ.* 78: 72–81.

Dubovik, O. and King M.D. (2000). A Flexible Inversion Algorithm for Retrieval of Aerosol Optical Properties from Sun and Sky Radiance Measurements. *J. Geophys. Res.* 105: 20673–20696.

Dubovik, O., Smirnov, A., Holben, B.N., King, M.D., Kaufman, Y.J., Eck, T.F. and Slutsker, I. (2000). Accuracy Assessments of Aerosol Optical Properties Retrieved from Aerosol Robotic Network (AERONET) Sun and Sky Radiance Measurements. *J. Geophys. Res.* 105: 9791–9806.

Dubovik, O., Holben, B.N., Eck, T.F., Smirnov, A., Kaufman, Y.J., King, M.D., Tanre, D. and Slutsker, I. (2002). Variability of Absorption and Optical Properties of Key Aerosol Types Observed in Worldwide Locations. *J. Atmos. Sci.* 59: 590–608.

Dubovik, O., Sinyuk, A., Lapyonok, T., Holben, B.N., Mishchenko, M., Yang, P., Eck, T.F., Volten, H., Muñoz, O., Veihelmann, B., van der Zande, W.J., Leon, J.F., Sorokin, M. and Slutsker, I. (2006). Application of Spheroid Models to Account for Aerosol Particle Nonsphericity in Remote Sensing of Desert Dust. *J. Geophys. Res.* 111: D11208.

Eck, T.F., Holben, B.N., Reid, J.S., Dubovik, O., Smirnov, A., O'Neill, N.T., Slutsker, I. and Kinne, S. (1999). Wavelength Dependence of the Optical Depth of Biomass Burning, Urban, and Desert Dust Aerosols. *J. Geophys. Res.* 104: 31333–31349.

Eck, T.F., Holben, B.N., Ward, D.E., Mukelabai, M.M., Dubovik, O., Smirnov, A., Schafer, J.S., Hsu, N.C., Piketh, S.J., Queface, A., Le Roux, J., Swap, R.J. and Slutsker, I. (2003). Variability of Biomass Burning Aerosol Optical Characteristics in Southern Africa during the SAFARI 2000 Dry Season Campaign and a Comparison of Single Scattering Albedo Estimates from Radiometric Measurements. *J. Geophys. Res.* 108: 8477.

Eck, T.F., Holben, B.N., Reid, J.S., Sinyuk, A., Hyer, E.J., O'Neill, N.T., Shaw, G.E., Vande Castle, J.R., Chapin, F.S., Dubovik, O., Smirnov, A., Vermote, E., Schafer, J.S., Giles, D., Slutsker, I., Sorokine, M. and Newcomb, W.W. (2009). Optical Properties of Boreal Region Biomass Burning Aerosols in Central Alaska and Seasonal Variation of Aerosol Optical Depth at an Arctic Coastal Site. *J. Geophys. Res.* 114: D11201.

Eck, T.F., Holben, B.N., Sinyuk, A., Pinker, R.T., Goloub, P., Chen, H., Chatenet, B., Li, Z., Singh, R.P., Tripathi, S.N., Reid, J.S., Giles, D.M., Dubovik, O., O'Neill, N.T., Smirnov, A., Wang, P. and Xia, X. (2010). Climatological Aspects of the Optical Properties of Fine/Coarse Mode Aerosol Mixtures. *J. Geophys. Res.* 115: D19205.

Feng, N. and Christopher, S.A. (2013). Satellite and Surface-based Remote Sensing of Southeast Asian Aerosols and

Their Radiative Effects. *Atmos. Res.* 122: 544–554.

Fu, J.S., Hsu, N.C., Gao, Y., Huang, K., Li, C., Lin, N.H. and Tsay, S.C. (2012). Evaluating the Influences of Biomass Burning during 2006 BASE-ASIA: A Regional Chemical Transport Modeling. *Atmos. Chem. Phys.* 12: 3837–3855.

Gautam, R., Hsu, N.C., Eck, T.F., Holben, B.N., Janjai, S., Jantarach, T., Tsay, S.C. and Lau, W.K. (2013). Characterization of Aerosols over the Indochina Peninsula from Satellite-surface Observations during Biomass Burning Pre-monsoon Season. *Atmos. Environ.* 78: 51–59.

Giles, D.M., Holben, B.N., Eck, T.F., Sinyuk, A., Smirnov, A., Slutsker, I., Dickerson, R.R., Thompson, A.M. and Schafer, J.S. (2012). An Analysis of AERONET Aerosol Absorption Properties and Classifications Representative of Aerosol Source Regions. *J. Geophys. Res.* 117: D17203.

Hao, W.M. and Liu, M.H. (1994). Spatial and Temporal Distribution of Tropical Biomass Burning. *Global Biogeochem. Cycles* 8: 495–503.

Hoffer, A., Gelencsér, A., Guyon, P., Kiss, G., Schmid, O., Frank, G.P., Artaxo, P. and Andreae, M.O. (2006). Optical Properties of Humic-like Substances (HULIS) in Biomass-burning Aerosols. *Atmos. Chem. Phys.* 6: 3563–3570.

Holben, B.N., Eck, T.F., Slutsker, I., Tanre, D., Buis, J.P., Setzer, A., Vermote, E., Reagan, J.A., Kaufman, Y.J., Nakajima, T., Lavenu, F., Jankowiak, I. and Smirnov, A. (1998). AERONET: A Federated Instrument Network and Data Archive for Aerosol Characterization. *Remote Sens. Environ.* 66: 1–16.

Holben, B.N., Tanré, D., Smirnov, A., Eck, T.F., Slutsker, I., Abuhassan, N., Newcomb, W.W., Schafer, J.S., Chatenet, B., Lavenu, F., Kaufman, Y.J., Castle, J.V., Setzer, A., Markham, B., Clark, D., Frouin, R., Halthore, R., Karneli, A., O'Neill, N.T., Pietras, C., Pinker, R.T., Voss, K., and Zibordi, G. (2001). An Emerging Ground-based Aerosol Climatology: Aerosol Optical Depth from AERONET. *J. Geophys. Res.* 106: 12067–12097.

Holben, B.N., Eck, T.F., Slutsker, I., Smirnov, A., Sinyuk, A., Schafer, J., Giles, D. and Dubovik, O. (2006). Aeronet's Version 2.0 Quality Assurance Criteria. *Proc. SPIE* 6408: 64080Q.

Hsu, N.C., Herman, J.R. and Tsay, S.C. (2003). Radiative Impacts from Biomass Burning in the Presence of Clouds during Boreal Spring in Southeast Asia. *Geophys. Res. Lett.* 30: 1224.

Huang, J., Hsu, N.C., Tsay, S.C., Jeong, M.J., Holben, B.N., Berkoff, T.A. and Welton, E.J. (2011). Susceptibility of Aerosol Optical Thickness Retrievals to Thin Cirrus Contamination during the BASE-ASIA Campaign. *J. Geophys. Res.* 116: D08214.

Kumar K.R., Sivakumar V., Reddy R.R., Gopal K.R. and Adesina A.J. (2014). Identification and Classification of Different Aerosol Types over a Subtropical Rural Site in Mpumalanga, South Africa: Seasonal Variations as Retrieved from the AERONET Sunphotometer. *Aerosol Air Qual. Res.* 14: 108–123.

Lee, D., Sud, Y.C., Oreopoulos, L., Kim, K.M., Lau, W.K. and Kang, I.S. (2014). Modeling the Influences of Aerosols on Pre-monsoon Circulation and Rainfall over Southeast Asia. *Atmos. Chem. Phys.* 14: 6853–6866.

Li, C., Tsay, S.C., Hsu, N.C., Kim, J.Y., Howell, S.G., Huebert, B.J., Ji, Q., Jeong, M.J., Wang, S.H., Hansell, R.A. and Bell, S.W. (2013). Characteristics and Composition of Atmospheric Aerosols in Phimai, Central Thailand during BASE-ASIA. *Atmos. Environ.* 78: 60–71.

Lin, N.H., Tsay, S.C., Reid, J.S., Yen, M.C., Sheu, G.R., Wang, S.H., Chi, K.H., Chuang, M.T., Ou-Yang, C.F., Fu, J.S., Lee, C.T.,Wang, L.C., Wang, J.L., Hsu, C.N., Holben, B.N., Chu, Y.C., Maring, H.B., Nguyen, A.X., Sopajaree, K., Chen, S.J., Cheng, M.T., Tsuang, B.J., Tsai, C.J., Peng, C.M., Chang, C.T., Lin, K.S., Tsai, Y.I., Lee, W.J., Chang, S.C., Liu, J.J. and Chiang, W.L. (2013). An Overview of Regional Experiments on Biomass Burning Aerosols and Related Pollutants in Southeast Asia: from BASE-ASIA and Dongsha Experiment to 7-SEAS. *Atmos. Environ.* 78: 1–19.

Lin, N.H., Sayer, A.M., Wang, S.H., Loftus, A.M., Hsiao, T.C., Sheu, G.R., Hsu, N.C., Tsay, S.C. and Chantara, S. (2014). Interactions between Biomass-burning Aerosols and Clouds over Southeast Asia: Current Status, Challenges, and Perspectives. *Environ. Pollut.* 195: 292–307.

More, S., Kumar, P.P., Gupta, P., Devara, P.C.S. and Aher, G.R. (2013). Comparison of Aerosol Products Retrieved from AERONET, MICROTOPS and MODIS over a Tropical Urban City, Pune, India. *Aerosol Air Qual. Res.* 13: 107–121.

Nodzu, M.I., Ogino, S., Tachibana, Y. and Yamanaka, M.D. (2006). Climatological Description of Seasonal Variations in Lower Tropospheric Temperature Inversions Layers over the Indochina Peninsula. *J. Clim.* 19: 3307–3319.

O'Neill, N.T., Eck, T.F., Smirnov, A., Holben, B.N. and Thulasiraman, S. (2003) Spectral Discrimination of Coarse and Fine Mode Optical Depth. *J. Geophys. Res.* 108: 4559.

Reid, J.S. and Hobbs, P.V. (1998). Physical and Optical Properties of Young Smoke from Individual Biomass Fires in Brazil. *J. Geophys. Res.* 103: 32013–32030.

Reid, J.S., Hyer, E.J., Johnson, R.S., Holben, B.N., Yokelson, R.J., Zhang, J., Campbell, J.R., Christopher, S.A., Di Girolamo, L., Giglio, L., Holz, R.E., Kearney, C., Miettinen, J., Reid, E.A., Turk, F.J., Wang, J., Xian, P., Zhao, G., Balasubramanian, R., Chew, B.N., Janjai, S., Lagrosas, N., Lestari, P., Lin, N.H., Mahmud, M., Nguyen, A.X., Norris, B., Oanh, N.T.K., Oo, M., Salinas, S.V., Welton, E.J. and Liew, S.C. (2013). Observing and Understanding the Southeast Asian Aerosol System by Remote Sensing: An Initial Review and Analysis for the Seven Southeast Asian Studies (7SEAS) Program. *Atmos. Res.* 122: 403–468.

Sharma, M., Kaskaoutis, D.G., Singh, R.P. and Singh, S. (2014). Seasonal Variability of Atmospheric Aerosol Parameters over Greater Noida Using Ground Sunphotometer Observation *Aerosol Air Qual. Res.* 14: 608–622.

Smirnov, A., Holben, B.N., Eck, T.F., Dubovik, O. and Slutsker, I. (2000). Cloud-Screening and Quality Control Algorithms for the AERONET Database. *Remote Sens.*

Environ. 73: 337–349.

Spinhirne, J.D., Rall, J.A.R. and Scott, V.S. (1995). Compact Eye Safe Lidar Systems. *Rev. Laser Eng.* 23: 112–118.

Streets, D.G., Yarber, K.F., Woo, J.H. and Carmichael, G.R. (2003). Biomass Burning in Asia: Annual and Seasonal Estimates and Atmospheric Emissions. *Global Biogeochem. Cycles* 17: 1099.

Tsai, J.H., Huang, K.L., Lin, N.H., Chen, S.J., Lin, T.C., Chen, S.C., Lin, C.C., Hsu, S.C. and Lin, W.Y. (2012). Influence of an Asian Dust Storm and Southeast Asian Biomass Burning on the Characteristics of Seashore Atmospheric Aerosols in Southern Taiwan. *Aerosol Air Qual. Res.* 15: 1105–1115.

Tsay, S.C., Hsu, N.C., Lau, W.K.M., Li, C., Gabriel, P.M., Ji, Q., Holben, B.N., Judd Welton, E., Nguyen, A.X., Janjai, S., Lin, N.H., Reid, J.S., Boonjawat, J., Howell, S.G., Huebert, B.J., Fu, J.S., Hansell, R.A., Sayer, A.M., Gautam, R., Wang, S.H., Goodloe, C.S., Miko, L.R., Shu, P.K., Loftus, A.M., Huang, J., Kim, J.Y., Jeong, M.J. and Pantina, P. (2013). From BASE-ASIA toward 7-SEAS: A Satellite-surface Perspective of Boreal Spring Biomass-burning Aerosols and Clouds in Southeast Asia. *Atmos. Environ.* 78: 20–34.

Wang, S.H., Tsay, S.C., Lin, N.H., Chang, S.C., Li, C., Welton, E.J., Holben, B.N., Hsu, N.C., Lau, W.K.M., Lolli, S., Kuo, C.C., Chia, H.P., Chiu, C.Y., Lin, C.C., Bell, S.W., Ji, Q., Hansell, R.A., Sheu, G.R., Chi, K.H. and Peng, C.M. (2013). Origin, Transport, and Vertical Distribution of Atmospheric Pollutants over the Northern South China Sea during the 7-SEAS/Dongsha Experiment. *Atmos. Environ.* 78: 124–133.

Welton, E.J., Voss, K.J., Gordon, H.R., Maring, H., Smirnov, A., Holben, B., Schmid, B., Livingston, J.M., Russell, P.B., Durkee, P.A., Formenti, P. and Andreae, M.O. (2000). Ground-based Lidar Measurements of Aerosols during ACE-2: Instrument Description, Results, and Comparisons with Other Ground-based and Airborne Measurements. *Tellus Ser. B* 52: 636–651.

Welton, E.J., Voss, K.J., Quinn, P.K., Flatau, P.J., Markowicz, K., Campbell, J.R., Spinhirne, J.D., Gordon, H.R. and Johnson, J.E. (2002). Measurements of Aerosol Vertical Profiles and Optical Properties during INDOEX 1999 Using Micropulse Lidars. *J. Geophys. Res.* 107: 8019.

Yen, M.C., Peng, C.M., Chen, T.C., Chen, C.S., Lin, N.H., Tzeng, R.Y., Lee, Y.A. and Lin, C.C. (2013). Climate and Weather characteristics in Association with the Active fires in Northern Southeast Asia and Spring Air Pollution in Taiwan during 2010 7-SEAS/Dongsha Experiment. *Atmos. Environ.* 78: 35–50.

Zhang, Y., Li, Z., Cuesta, J., Li, D., Wei, P., Xie, Y. and Li, L. (2015). Aerosol Column Size Distribution and Water Uptake Observed during a Major Haze Outbreak over Beijing on January 2013. *Aerosol Air Qual. Res.* 15: 945–957.

Received for review, May 13, 2015
Revised, August 5, 2015
Accepted, August 11, 2015